MONTHLY PROGRESS REPORT NO. 13
FOR JUNE 1984
SRB/FWC WATER IMPACT - FLEXIBLE BODY LOADS TEST

July 1984

Prepared for:

Dennis Kross, ED22
National Aeronautics and Space Administration
George C. Marshall Space Flight Center
Marshall Space Flight Center, AL 35812

Prepared by:

Bolt Beranek and Newman Inc.
10 Moulton Street
Cambridge, MA 02238

During June, the work performed focused on means for simplifying the modeling of the cavity collapse pressure loading. Although there is currently some concern that all of the pressure data obtained during the quarter scale tests at NSWC may be contaminated with case strain effects, ultimately we will have to use scaled-up 8% and full scale cavity collapse pressure data to estimate the response of the full scale FWC/SRB to cavity collapse loads. Since the pressure field on the SRB during cavity collapse is quite complex and the number of pressure transducers is usually limited, means must be found for extracting the maximum information from the available data or for synthesizing a valid but simple model of the pressure loading function.

If one examines the output of the 22 pressure sensors on the quarter scale model during cavity collapse, it is difficult to see any pattern in the pressure loading. Fortunately, there are excellent high speed color films of the quarter scale model during cavity collapse. In these films, it is possible to see a very clearly defined pressure wave front propagating circumferentially around the vehicle that seems to be associated at least on the lee side, with an abrupt rise in pressure at each pressure transducer.

By using a motion analyzer and stepping through the films, we have traced out the location of this wave front at a number of time intervals for drops 17 through 21. The picture that emerges is remarkably similar for each drop. Figures 1 through 5 show the wave fronts at 16 msec (4 frame) intervals traced out on a scaled drawing of the quarter scale test fixture. Figure 1, for example, shows nine different wave fronts. the first wave that is visible on the keel side of the vehicle (the righthand side of the test fixture in Fig. 1 and subsequent figures). As time passes, the wave front moves to the left in the figure and

circumferentially around the vehicle. Although we cannot see it, we would assume that there is a symmetric wave front on the opposite side of the vehicle also propagating circumferentailly around the vehicle. The two wave fronts then meet on the lee side of the vehicle and generate the large pressures associated with cavity collapse.

Table 1 shows the entry conditions for the five drops that have been examined so far. Also shown is the average wave front velocity for each drop, based on 56.5 in. (half the circumference of the test article) divided by the total traverse time.

TABLE 1 ENTRY CONDITIONS AND WAVEFRONT VELOCITIES FOR DROPS 17-21

Drop No.	Entry Velocity	Entry Angle	Avg. Wavefront Velocity
17	32.5 ft/sec	3.5°	32.6 ft/sec
18	37.5 ft/sec	3.5°	49.0 ft/sec
19	37.5 ft/sec	3.5°	49.0 ft/sec
20	37.5 ft/sec	6.25°	36.8 ft/sec
21	42.5 ft/sec	3.75°	58.8 ft/sec

Examining Figs. 1 through 5 and Table 1, we can come to a number of qualitative conclusions regarding the modeling of the applied cavity collapse loads.

First, between stations 30 and 60 on the test article, the wave front propagates circumferentially around the cylinder. To first order that wave front can be thought to be nearly straight and parallel to the cylinder axis. This simple picture of the cavity collapse pressure can be very helpful in reconstructing the spatial distribution of the pressure. For example, if one knows the pressure time history at a given circumferential

location θ_o, one can construct from that time history the spatial distribution of the pressure about θ_o. To do so, one makes the approximation that for some limited region around a given pressure transducer the pressure distribution is a circumferentially traveling pressure wave

$$P(\theta,t) \simeq P(\theta - \frac{Vt}{R}) \tag{1}$$

where θ is the circumferential angle, t is time, V is the speed of the pressure wave and R is the cylinder radius. If we have the time history of the pressure from a pressure transducer at θ_o, we can transform that into a snapshot of the spatial pressure distribution at any time t_o through a simple coordinate transformation. We simply recognize that as long as the argument of Eq. 1, $(\theta - \frac{Vt}{R})$, is the same value, the pressure will be the same, e.g.,

$$P(\theta,t_o) = P(\theta_o,t) \tag{2}$$

if

$$\theta - \frac{Vt_o}{R} = \theta_o - \frac{Vt}{R} \tag{3}$$

or if,

$$\theta-\theta_o = \frac{V}{R}(t - t_o) \tag{4}$$

Equation 4 allows us to make a one to one correspondence between time t and spatial position θ. We have done just that in Fig. 6 with the output of pressure transducers P7 and P9 in drop 18 using V = 49 ft/sec, as obtained from the films. Figure 6 shows the two traveling waves converging on one another with the likely meeting point near transducer P8 where the maximum pressure was observed.

This technique offers a powerful means for estimating pressures at circumferential positions where we have limited pressure transducers. Of course it must be applied with some care. Equation 1 assumes that the pressure trace does not change as it propagates around the cylinder. In fact we know that the pressure trace does change as it moves from the keel to the lee side. Consequently, we can only do the extrapolation in Eq. 4 in a limited region to each side of a pressure transducer. In any event, applying this technique will enable us to obtain a considerably more detailed circumferential pressure distribution that we could otherwise obtain. In addition, since the wave fronts are nearly parallel to the cylinder axis, linear interpolation in the axial direction will probably provide adequate detail.

A second qualitative conclusion concerns the duration of the pressure wave in both space and time. Table 1 shows that the wave front propagates very slowly taking nearly 100 msec to go from the keel side of the vehicle to the lee side. That time period is long compared to any of the natural periods of the test fixture. Consequently modeling the pressure input as impulsive in time would result in erroneous predictions. We encounter similar problems if we try to model the cavity collapse pressure as an impulse traveling circumferentially around the cylinder. Figure 6 shows that rather than being confined to a limited portion of the circumference of the cylinder, the pressure is significant over nearly a quarter of the circumference. Consequently, modeling the pressure wave as implusive in space will also be incorrect.

FIGURE 1

DROP 17

first front 117 frames

after water impact

each front 4 frames

56.5 in around

V_f = 32.6 ft/sec

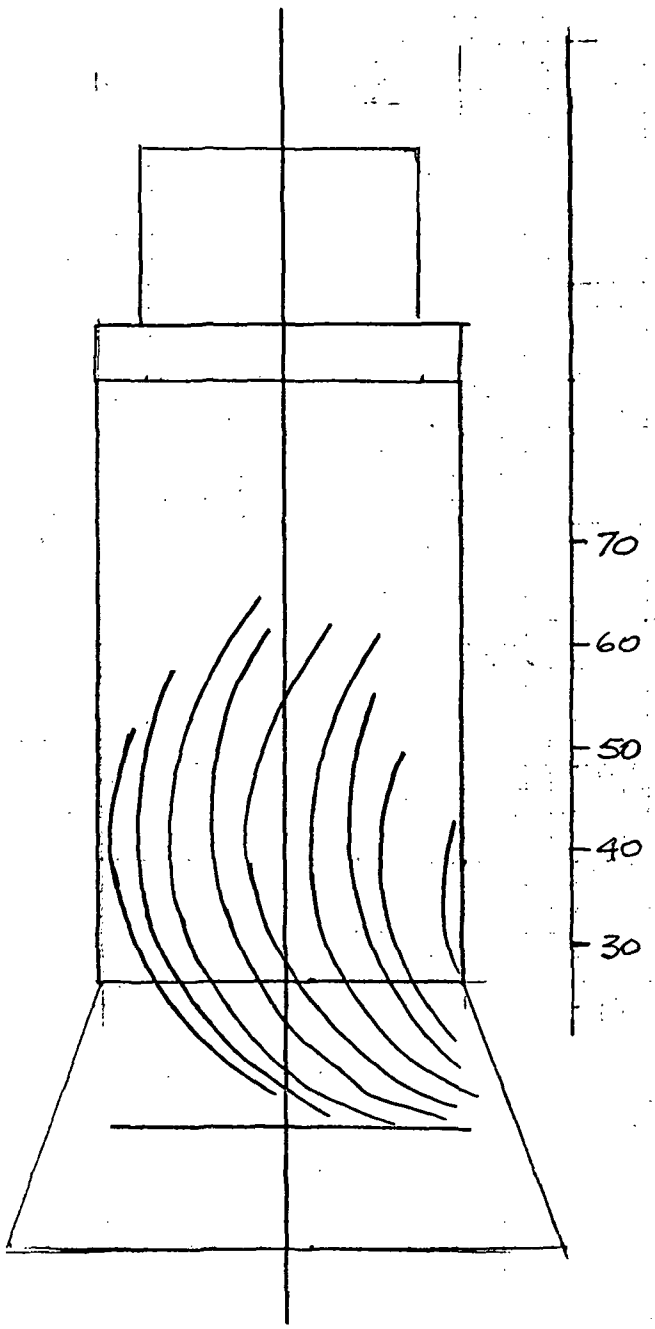

FIGURE 2
DROP 18
first front 117 frames
after WATER impact
each front 4 frames
V_f 49.0 ft/sec

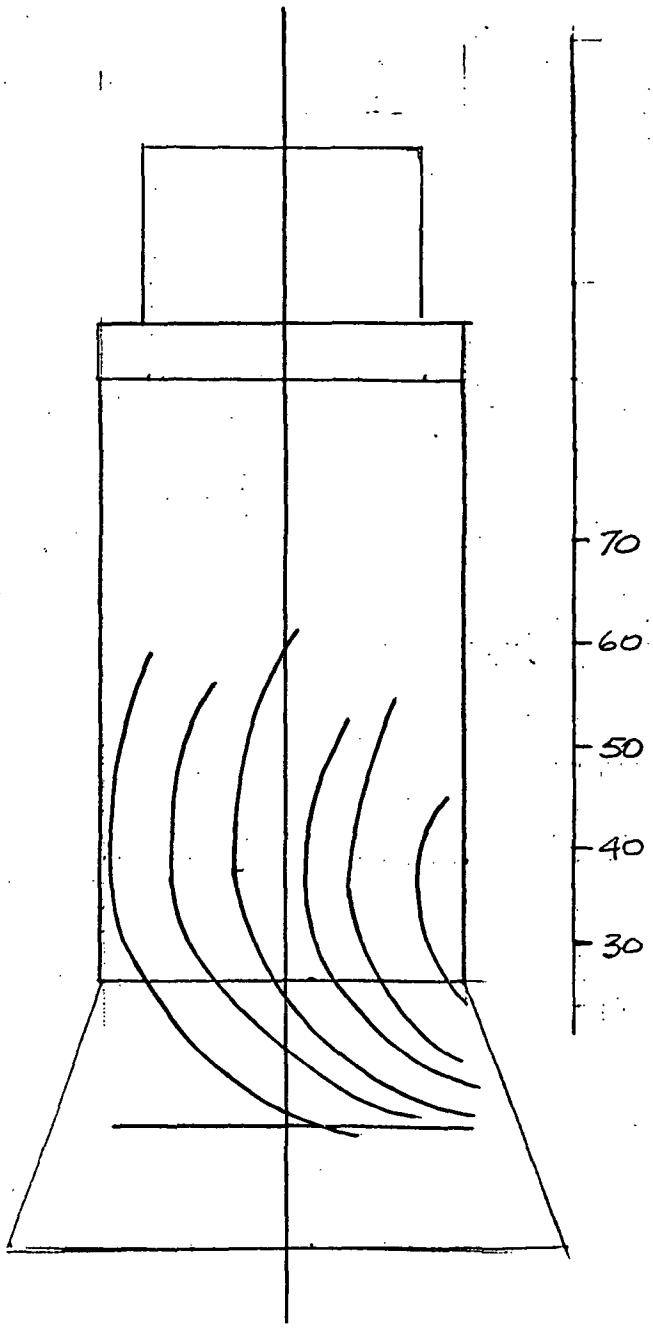

FIGURE 3
DROP 19

first front 119 frames
after water impact
each front 4 frames

V_f = 49.0 ft/sec

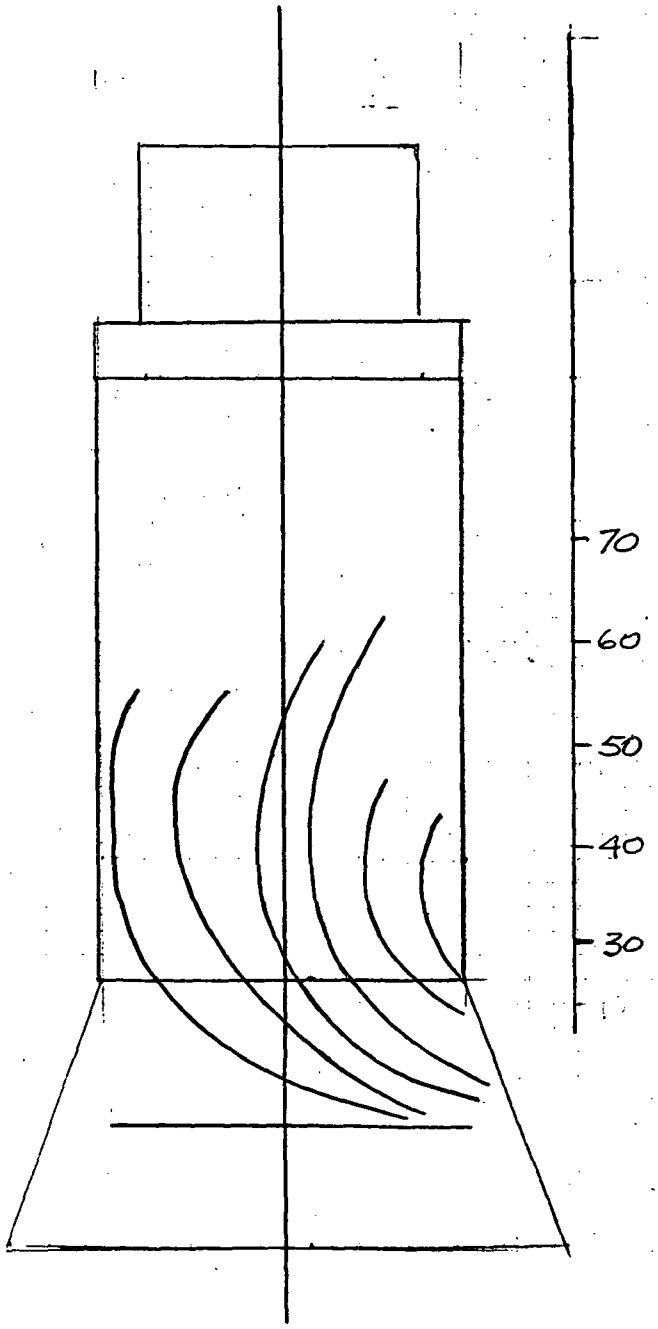

FIGURE 4.
DROP 20

first front 108 frames

After water impact

each front 4 frames

V_f = 36.8 ft/sec

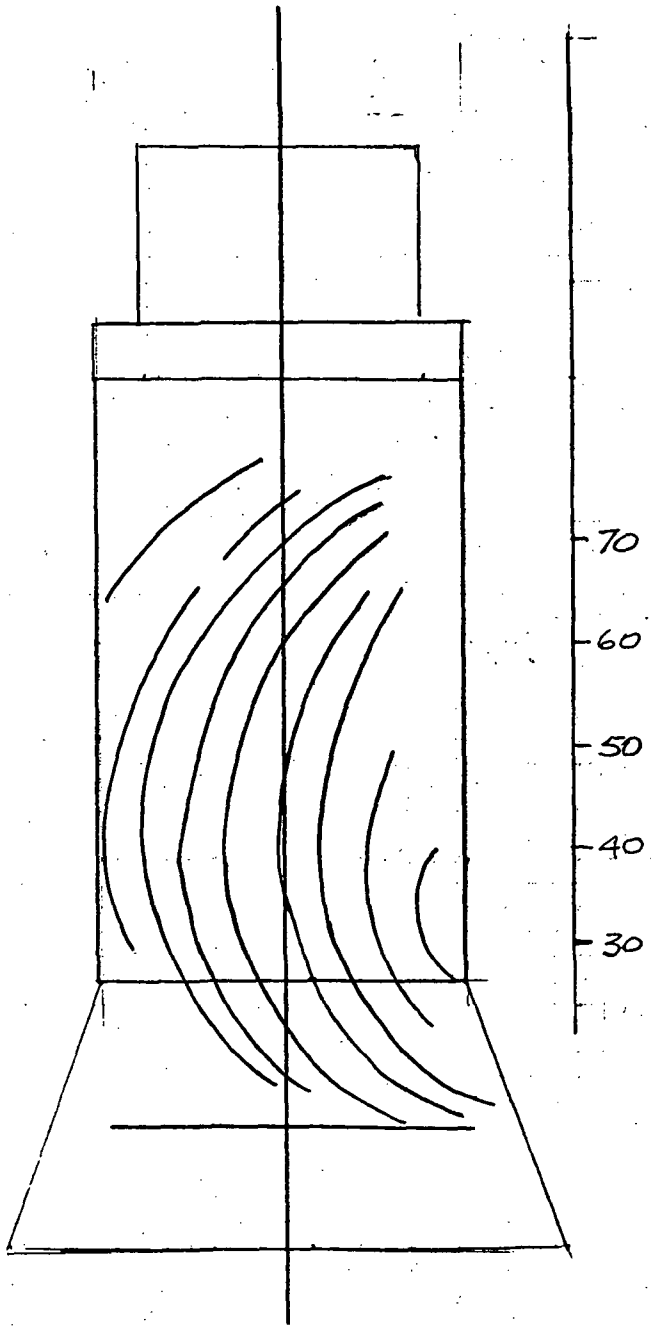

FIGURE 5
DROP 21

first front 125 frames
after water impact
each front 4 frames
V_f = 58.3 ft/sec

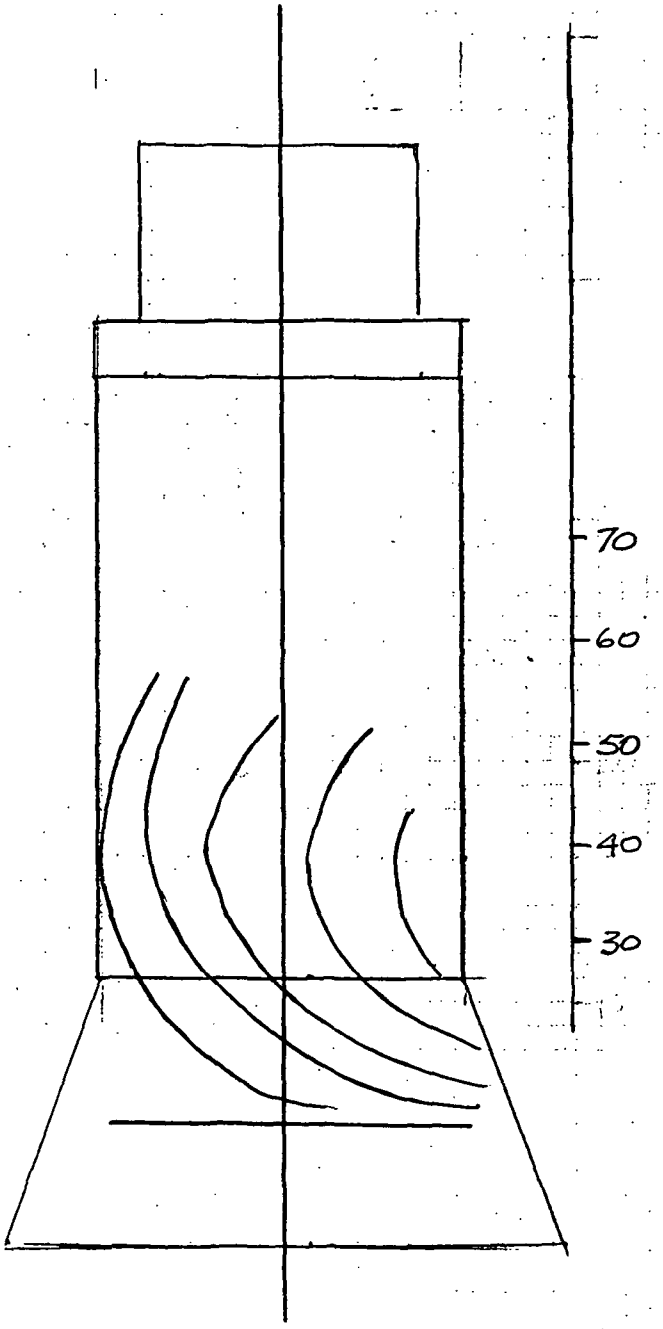

PRESSURE WAVE
DROP 18

STA: 42.5

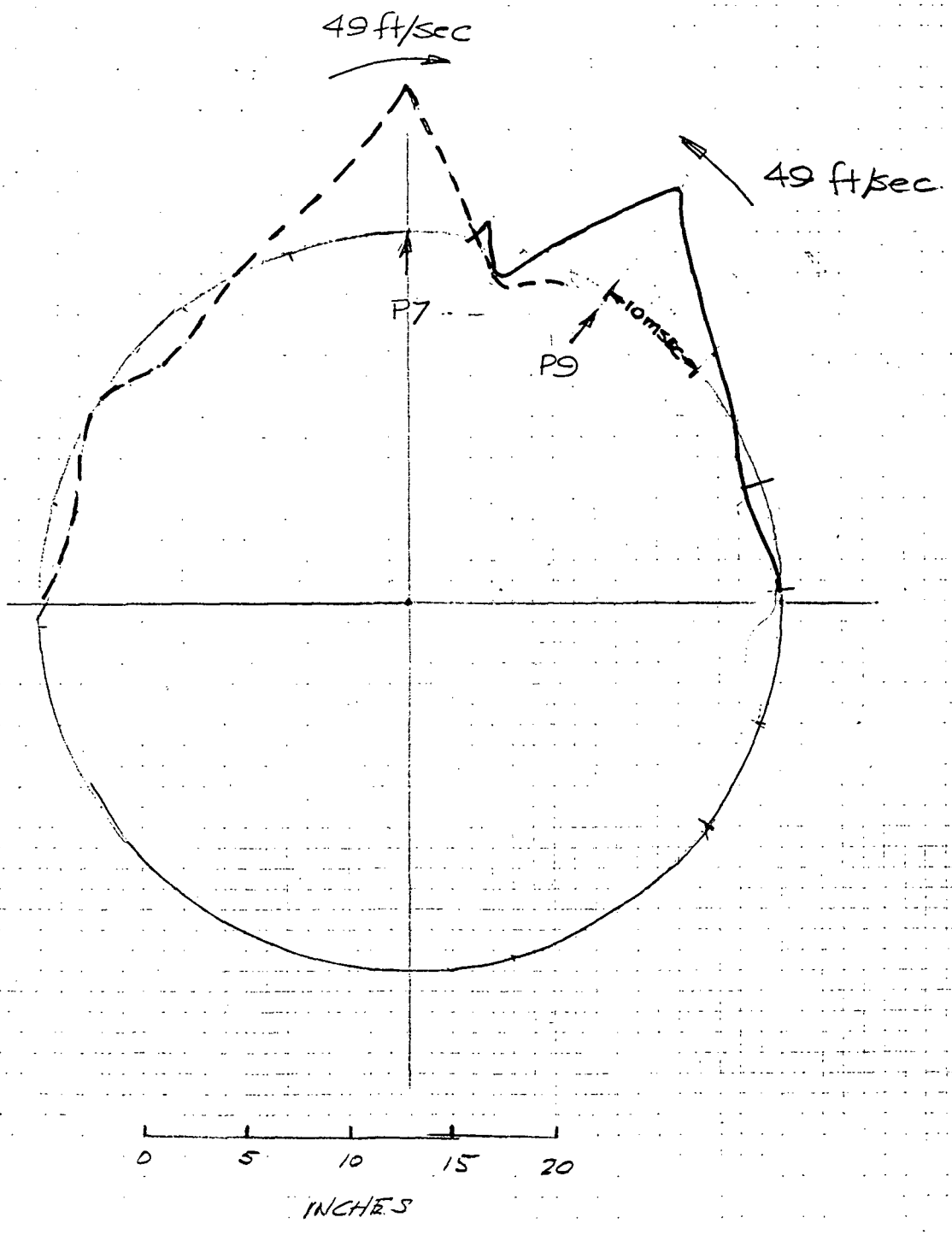

FIGURE 6